Journal of Chromatography A, 1216 (2009) 1084–1093

Contents lists available at ScienceDirect

Journal of Chromatography A

journal homepage: www.elsevier.com/locate/chroma

Extra-column dead volume in simulated moving bed separations: Theory and experiments

Shigeharu Katsuo[a,1], Christian Langel[a], Patrick Schanen[b], Marco Mazzotti[a,*]

[a] Institute of Process Engineering, ETH Zurich, Sonneggstrasse 3, CH-8092 Zurich, Switzerland
[b] Laboratory of Organic Chemistry, ETH Zurich, Wolfgang-Paulistrasse 10, CH-8093 Zurich, Switzerland

ARTICLE INFO

Article history:
Received 14 July 2008
Received in revised form 8 December 2008
Accepted 15 December 2008
Available online 24 December 2008

Keywords:
Simulated moving bed chromatography
Extra-column dead volume
Chiral chromatography
(±)-3,5-Bis[1-(4-methoxyphenyl)-1-methyl]hepta-3,4-diene-1,6-diyne

ABSTRACT

In small-scale SMB units typically set up by a number of HPLC columns connected in series, the volume of the connecting tubing parts and valves may become comparable to the column volume. Therefore, to guarantee proper and satisfying separation results, the introduced extra-column dead volume needs to be considered in the calculations of the operating parameters. In this work, the impact of extra-column dead volume on the separation performance is studied, with the objective to introduce guidelines and rather simple rules to account for it. It is shown, how these results can be used in the frame of the triangle theory to determine operating conditions that allow to achieve the desired separation performance. For the experiments the separation of a racemic mixture of (±)-3,5-bis[1-(4-methoxyphenyl)-1-methyl]hepta-3,4-diene-1,6-diyne was carried out. The numerical model used for the simulation describes explicitly the geometric configuration of the HPLC–SMB laboratory unit to take into account the effect of extra-column dead volume.

1. Introduction

Laboratory and small-scale simulated moving bed (SMB) units consist of high-performance liquid chromatography (HPLC) columns connected in series, where the associated extra-column dead volume connecting columns and valves may become comparable to the column volume. In these cases, the extra-column dead volume has to be taken into account in the design and simulation of SMB separations to guarantee proper and satisfactory operating conditions. This issue has been mentioned and discussed in previous works [1–3]. The effect of extra-column dead volume on the retention time of the compounds to be separated was studied, and it was demonstrated how to account for it in the calculation of the SMB operating parameters [3]. Later a formula was proposed to determine the dead volume for the different sections of an existing unit [4,5]. According to this formula, the dead volume for the different sections is obtained by dividing the overall extra-column dead volume of one section by the number of columns in this section. More recently, we have reached the conclusion that such a formula is not correct. Therefore, the objective of this work is to present guidelines to determine the extra-column dead volume for the different sections of an SMB unit and to discuss its effect on the separation performance.

In the first part of the paper a general rule to account for the extra-column dead volume is derived. In the following its effect is analyzed and discussed through simulations making use of a model that accounts for the extra-column dead volume based on the exact geometric configuration of the laboratory SMB unit. In addition, the conclusions are supported experimentally through results obtained in the separation of a racemic mixture of (±)-3,5-bis[1-(4-methoxyphenyl)-1-methyl]hepta-3,4-diene-1,6-diyne, also referred to as allene [6–9]. The obtained experimental data are compared to the simulation results and the effect of extra-column dead volume on the separation is presented in the frame of the "Triangle Theory" [10,11].

2. HPLC–SMB unit

2.1. SMB unit

In Fig. 1, a schematic of our laboratory four-section SMB unit in the 2-2-2-2 configuration is shown, with the inlet (Feed F, and Desorbent D) and outlet ports (Raffinate R, Extract E, and Outlet O). Note that in Fig. 1, the possibility of an open or closed loop system is considered. In the latter case, the stream recovered at the Outlet port of the last column of Section 4 is mixed before the inlet of the recycling pump with fresh desorbent and fed back to the first column of Section 1, whereas in the former case, the stream is

* Corresponding author. Tel.: +41 44 632 24 56, fax: +41 44 632 11 41.
E-mail address: marco.mazzotti@ipe.mavt.ethz.ch (M. Mazzotti).
[1] Permanent address: Mitsubishi Chemical Group Science and Technology Research Center, Inc., 1000 Kamoshida-cho, Aoba-ku, Yokohama 227-8502, Japan.

0021-9673/$ – see front matter © 2008 Elsevier B.V. All rights reserved.
doi:10.1016/j.chroma.2008.12.031

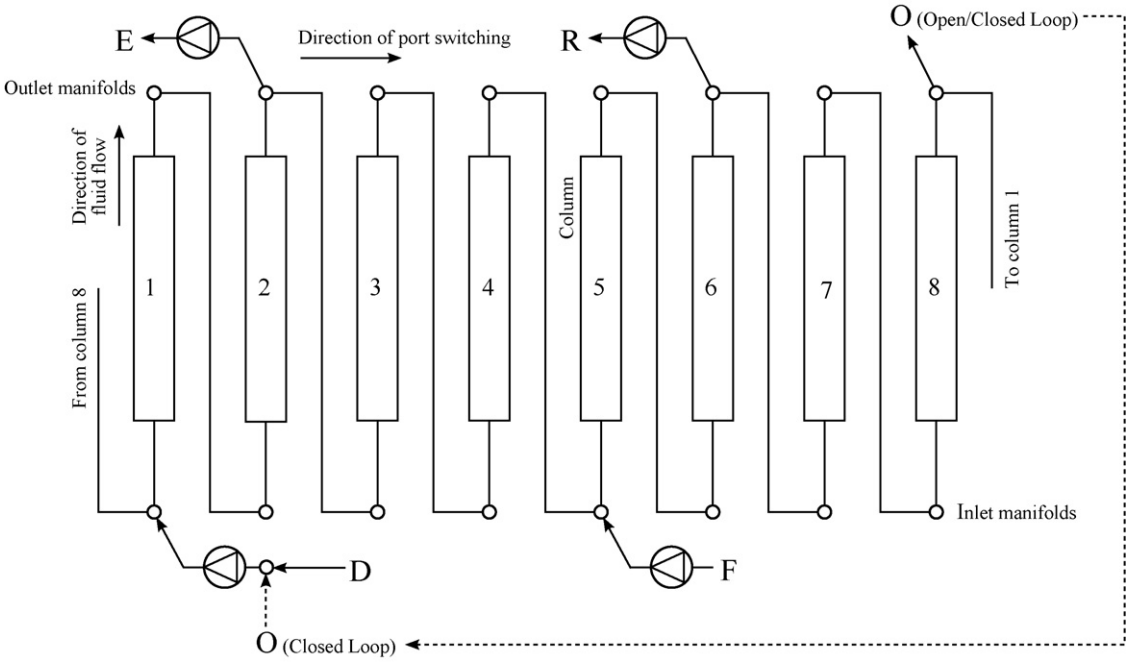

Fig. 1. Scheme of the 2-2-2-2 laboratory scale SMB unit.

completely withdrawn at the Outlet port. In this configuration the recycling pump is not part of the SMB loop, hence the volume containing the recycling pump and the related tubing is not relevant for the dead volume considerations. However, the tubing connecting the last column of the loop to the first is indeed part of the loop, but since the pressure at the Desorbent port is larger than that at the Outlet port there is no flow in that tubing.

Our unit represents only one of the possible implementations of an SMB system, and the port configuration is one among all conceivable ones illustrated in Fig. 2. The two inlet and three outlet streams are not labeled explicitly, since their relative position can be chosen arbitrarily as far as the analysis below is concerned. If in the following discussion it is needed to define a certain port explicitly, the notation shown in Fig. 2(c) will be used. The volume of the tubing connecting an inlet port (D or F) to a column inlet is indicated as $V_{\mathrm{p}}^{\mathrm{i}}$ (p = D,F), whereas the one connecting the column outlet to an outlet port (E, R or O) is $V_{\mathrm{p}}^{\mathrm{o}}$ (p = E,R,O). The set of tubing connecting two successive columns, i.e. between the previous column's outlet and the next column's inlet, has the same volume V^{D}.

An important alternative implementation of the SMB technology is commercialized by the French company, Novasep, where the recycling pump is part of the SMB loop and its presence is compensated by an asynchronous switch of the inlet and outlet ports [12,13]. This case is not among these considered here.

2.2. Mathematical model and numerical method

In this work the SMB unit is viewed as an assemble of chromatographic columns separated by pieces of tubing, according to the relevant port location, i.e. one of these in Fig. 2. Depending on the relevant outlet and inlet flows, the different tubing pieces experience different flow rates, which affect the residence time accordingly.

For the chromatographic column we use the equilibrium-dispersive model, hence the mass balance for component i can be written as [3,14–16]:

$$\epsilon^* \frac{\partial c_i}{\partial t} + (1-\epsilon^*)\frac{\partial n_i^*}{\partial t} + u\frac{\partial c_i}{\partial z} = \epsilon^* D_{\mathrm{ap},i}\frac{\partial^2 c_i}{\partial z^2} \quad (i = \mathrm{A,B}). \tag{1}$$

The right-hand side of the equation accounts for axial dispersion and mass-transfer resistance, lumped together in an apparent dispersion coefficient, $D_{\mathrm{ap},i}$. In Eq. (1), c_i and n_i^* are mobile phase and equilibrium stationary phase concentration, respectively. The phase equilibrium between the fluid and the adsorbed phase is characterized by the adsorption isotherm $n_i^* = f_i(c_{\mathrm{A}}, c_{\mathrm{B}})$. Moreover, ϵ^* is the overall bed void fraction and u is the superficial velocity of the fluid. The Danckwerts boundary conditions are implemented:

$$\epsilon^* D_{\mathrm{ap},i}\left.\frac{\partial c_i}{\partial z}\right|_{z=0} = u(\left. c_i\right|_{z=0} - \phi_i^{\mathrm{OUT}}(t)), \qquad \left.\frac{\partial c_i}{\partial z}\right|_{z=L} = 0, \tag{2}$$

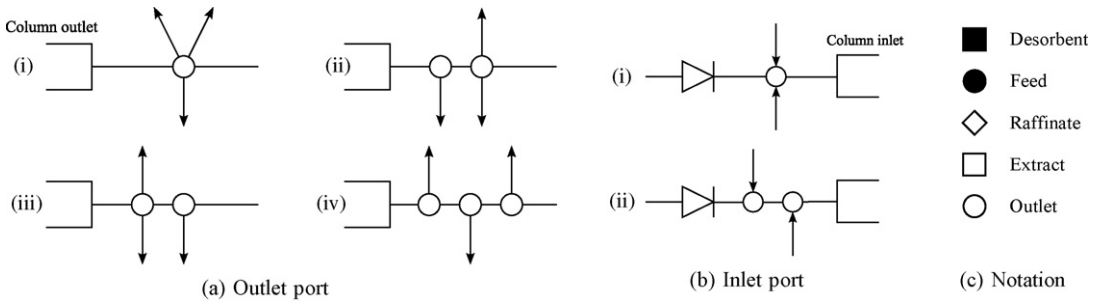

Fig. 2. Illustration of the different possible outlet and inlet port configurations.

where $\phi_i^{\mathrm{OUT}}(t)$ is the concentration profile at the outlet of the preceding piece of tubing.

In order to solve Eq. (1) numerically, the finite difference method is applied. Using a first-order backward difference to discretize the first-order space derivative in Eq. (1) leads to the following relationship:

$$\frac{c_i(z)-c_i(z-\Delta z)}{\Delta z} = \left.\frac{\partial c_i}{\partial z}\right|_z - \left.\frac{\partial^2 c_i}{\partial z^2}\right|_z \frac{\Delta z}{2} + O(\Delta z^2), \tag{3}$$

with $\Delta z > 0$ representing the space grid size. The numerical error introduced by neglecting the second term on the right-hand side of Eq. (3) yields a numerical dispersion corresponding to a dispersion coefficient:

$$D_{\mathrm{num}} = \frac{u\Delta z}{2\epsilon^*}. \tag{4}$$

Therefore, in the numerical calculations the apparent dispersion coefficients were corrected using numerical dispersion, thus yielding:

$$\tilde{D}_{\mathrm{ap},i} = D_{\mathrm{ap},i} - D_{\mathrm{num}} \quad (i = \mathrm{A,B}). \tag{5}$$

The space grid size Δz was chosen so as to fulfill the condition $\Delta z < 2\epsilon^* D_{\mathrm{ap},i}/u$, which depends on the superficial velocity u. In this work Δz was chosen to be $L/500$ or $L/600$.

Each piece of tubinh that is part of the extra-column dead volume can be described using a conventional diffusion model:

$$\frac{\partial c_i}{\partial t} + u^{\mathrm{D}}\frac{\partial c_i}{\partial z} = D_i^{\mathrm{D}}\frac{\partial^2 c_i}{\partial z^2}. \tag{6}$$

In Eq. (6), u^{D} and D_i^{D} are the superficial velocity of the fluid and the dispersion coefficient of each component in the tubing, respectively. The boundary conditions for the tubing are given by

$$c_i(t,0) = \phi_i^{\mathrm{IN}}(t), \quad \left.\frac{\partial c_i}{\partial z}\right|_{z=L^{\mathrm{D}}} = 0, \tag{7}$$

where $\phi_i^{\mathrm{IN}}(t)$ and L^{D} are the concentration profile at the inlet of the tubing and the tubing length, respectively. The variable $\phi_i^{\mathrm{IN}}(t)$ equals $\phi_i^{\mathrm{OUT}}(t)$ always, but in the case of the tubing immediately following Desorbent or Feed port, the following equations apply:

$$\phi_i^{\mathrm{IN,D}}(t) = \begin{cases} \dfrac{Q_4}{Q_1}\phi_i^{\mathrm{OUT}}(t) & \text{closed loop,} \\ 0 & \text{open loop,} \end{cases}$$
$$\phi_i^{\mathrm{IN,F}}(t) = \frac{Q_2\phi_i^{\mathrm{OUT}}(t) + (Q_3 - Q_2)c_{i,\mathrm{F}}}{Q_3}, \tag{8}$$

where Q_j is the flow rate in section j. The first-order backward difference introduces a numerical error that can be adjusted to be proportional to the second-order term on the right-hand side of Eq. (6). Therefore, the dispersion effects in the extra-column dead volume are only described in terms of numerical dispersion, which corresponds to saying that

$$D_i^{\mathrm{D}} = \frac{1}{2}u^{\mathrm{D}}\,\Delta z^{\mathrm{D}}, \tag{9}$$

with Δz^{D} being the space grid size used in the simulation. In this work a large number of grid points is desirable to minimize the effect of back-mixing in the tubing due to numerical dispersion and to focus on the role of the extra tubing in the frame of the triangle theory, i.e. the change in residence time [3]. Therefore, Δz^{D} was chosen as the tubing length corresponding to a volume of 0.001 mL.

The model of the SMB unit with extra-column dead volume is then formulated with the above-mentioned differential-algebraic equations (DAEs). The numerical solution is obtained using a DAE solver with backward differentiation formula (BDF).

3. Extra-column dead volume

3.1. Accounting for the dead volume

Comparing an SMB unit with and without extra-column dead volume, it is obvious that the extra tubing leads to an increase of the residence time of the species to be separated, as discussed earlier [3].

For the sake of simplicity but without lose of generality [3], let us consider two components A and B, subject to the linear isotherms:

$$n_i = H_i C_i \qquad (i = \mathrm{A,B}), \tag{10}$$

with $H_{\mathrm{A}} > H_{\mathrm{B}}$. For any SMB operation, one can determine constraints for complete separation of the components in Sections 2 and 3, and regeneration of the stationary and mobile phase in Sections 1 and 4, respectively. The constraints can be expressed in terms of residence time, which can be calculated as

$$\bar{t}_{i,j}^{\mathrm{r}} = t_j^{\mathrm{D}} + t_{i,j}^{\mathrm{r}} = \frac{V_j^{\mathrm{D}}}{Q_j} + \frac{V\epsilon^*}{Q_j}\left[1 + \frac{(1-\epsilon^*)}{\epsilon^*}H_i\right] \quad (i = \mathrm{A,B};\ j = 1,\ldots,4), \tag{11}$$

where V is the column volume, V_j^{D} the dead volume that applies to section j and will be specified later, and Q_j is the fluid flow rate in section j. Eq. (11) consists of two terms, the first being the residence time of component i in the extra-column dead volume of section j, and the second its retention time in the chromatographic column. For complete separation, it is required that the following constraints be fulfilled [3]:

$$\begin{aligned} &\text{Section 1}: && \bar{t}_{\mathrm{A},1}^{\mathrm{r}} \le t^*, \\ &\text{Section 2}: && \bar{t}_{\mathrm{B},2}^{\mathrm{r}} \le t^* \le \bar{t}_{\mathrm{A},2}^{\mathrm{r}}, \\ &\text{Section 3}: && \bar{t}_{\mathrm{B},3}^{\mathrm{r}} \le t^* \le \bar{t}_{\mathrm{A},3}^{\mathrm{r}}, \\ &\text{Section 4}: && t^* \le \bar{t}_{\mathrm{B},4}^{\mathrm{r}}. \end{aligned} \tag{12}$$

The effective flow rate ratio $\bar{m}_j$ takes into account the extra-column dead volume and is defined as follows [3]:

$$\bar{m}_j = m_j - m_j^{\mathrm{D}} = \frac{Q_j t^* - V\epsilon^*}{V(1-\epsilon^*)} - \frac{V_j^{\mathrm{D}}}{V(1-\epsilon^*)}. \tag{13}$$

Substituting Eqs. (11) and (13) into inequalities (12) yields the following constraints on the parameters $\bar{m}_j$:

$$\begin{aligned} &H_{\mathrm{A}} \le \bar{m}_1, \\ &H_{\mathrm{B}} \le \bar{m}_2 \le H_{\mathrm{A}}, \\ &H_{\mathrm{B}} \le \bar{m}_3 \le H_{\mathrm{A}}, \\ &\bar{m}_4 \le H_{\mathrm{B}}. \end{aligned} \tag{14}$$

It is obvious from Eq. (13) that whenever the extra-column dead volume V_j^{D} becomes very small compared to the column volume V its effect can be neglected.

3.2. Calculating the extra-column dead volume

In this section, V_j^{D} is specified for all different SMB sections as well as for all possible column configurations (n_1-n_2-n_3-n_4), where n_j is the number of columns in section j.

3.2.1. Section 1

In Section 1 the stationary phase needs to be regenerated completely and no A should be brought to Section 4 with the next switch. Considering the case of two or more columns in Section 1, as shown in Fig. 3(a), it can readily be seen that during the time interval between two port switches component A needs to be removed between ports p_1 and p_2 to fulfill this constraint. Therefore, the

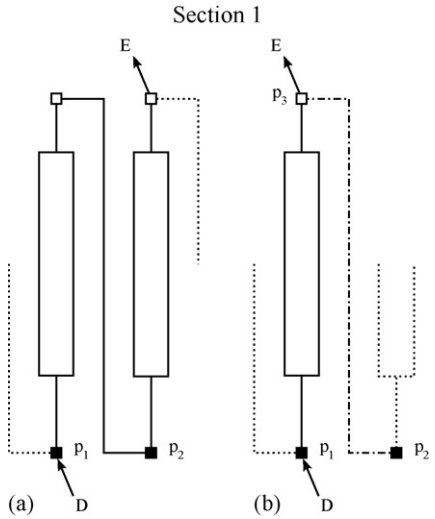

Fig. 3. Scheme of Section 1 for different column configurations: (a) two columns; (b) one column.

switching time t^* should be larger than the residence time of the more retained component A in that section of the SMB, i.e.

$$t^* \geq t^{\mathrm{r}}_{\mathrm{A},1}(\mathrm{p}_1 \text{ to } \mathrm{p}_2), \tag{15}$$

where $t^{\mathrm{r}}_{i,j}(\mathrm{p}_1 \text{ to } \mathrm{p}_2)$ (i = A,B) is the traveling time of species i from p_1 to p_2 at the flow rate prevailing in section j, i.e. Q_j. If there is only one column in Section 1, as shown in Fig. 3(b), component A still needs to be removed between p_1 and p_2. However, the flow rate is no longer constant between p_1 and p_2 but it is Q_1 between p_1 and p_3 and Q_2 between p_3 and p_2. Hence, the requirement for complete regeneration in terms of residence time is given by

$$t^* \geq t^{\mathrm{r}}_{\mathrm{A},1}(\mathrm{p}_1 \text{ to } \mathrm{p}_3) + t^{\mathrm{r}}_{\mathrm{A},2}(\mathrm{p}_3 \text{ to } \mathrm{p}_2). \tag{16}$$

3.2.2. Section 2

Fig. 4 illustrates the case where Section 2 has two or more columns, Fig. 4(a), and that where it has one column only, Fig. 4(b). Pure A should be recovered from the Extract port, and to meet this requirement, in the moment of the switch no B should be left in the SMB section between ports p_1 and p_2. On the other hand, to make sure that it can be obtained at the Extract port, A should not be moved beyond port p_2. Hence, the constraint for the switching time t^* can be written as

$$t^{\mathrm{r}}_{\mathrm{B},2}(\mathrm{p}_1 \text{ to } \mathrm{p}_2) \leq t^* \leq t^{\mathrm{r}}_{\mathrm{A},2}(\mathrm{p}_1 \text{ to } \mathrm{p}_2). \tag{17}$$

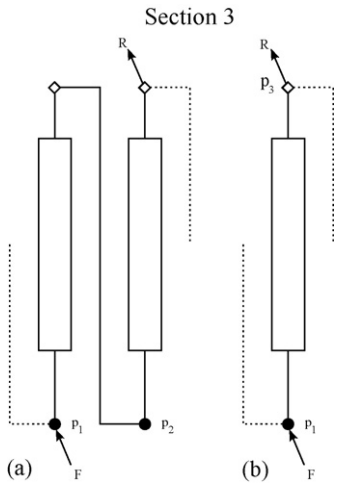

Fig. 5. Scheme of Section 3 for different column configurations: (a) two columns; (b) one column.

3.2.3. Section 3

In Section 3 pure B should be recovered at the Raffinate port. For the configurations where two or more columns are present in Section 3, it can readily be seen from Fig. 5(a) that the switching time t^* should be larger than the residence time of B and smaller than the one of A between ports p_1 and p_2. This leads to

$$t^{\mathrm{r}}_{\mathrm{B},3}(\mathrm{p}_1 \text{ to } \mathrm{p}_2) \leq t^* \leq t^{\mathrm{r}}_{\mathrm{A},3}(\mathrm{p}_1 \text{ to } \mathrm{p}_2). \tag{18}$$

Fig. 5(b) illustrates the situation where Section 3 consists of only one column. In order to get pure Raffinate at the Raffinate port, component A should not reach the Raffinate port hence the constraint reads as follows:

$$t^{\mathrm{r}}_{\mathrm{B},3}(\mathrm{p}_1 \text{ to } \mathrm{p}_3) \leq t^* \leq t^{\mathrm{r}}_{\mathrm{A},3}(\mathrm{p}_1 \text{ to } \mathrm{p}_3). \tag{19}$$

3.2.4. Section 4

Operating a closed loop system, the mobile phase needs to be regenerated in Section 4 to avoid pollution of Section 1 with compo-

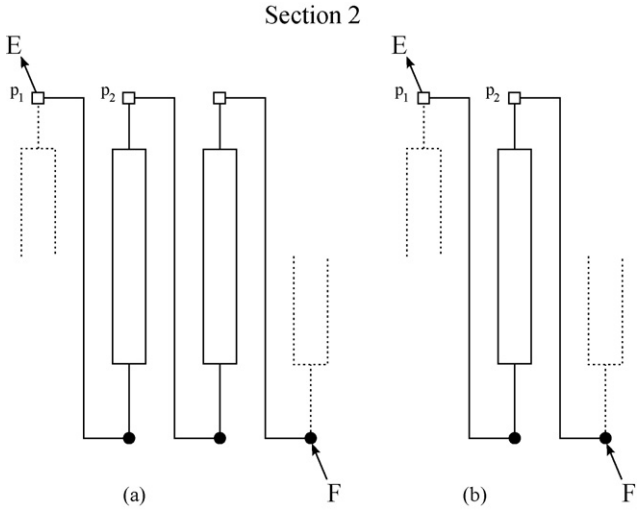

Fig. 4. Scheme of Section 2 for different column configurations: (a) two columns; (b) one column.

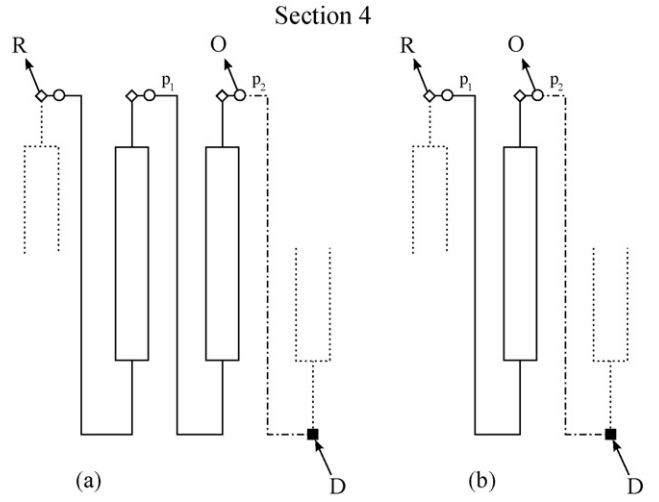

Fig. 6. Scheme of Section 4 where the O port is positioned *after* the R port: (a) two columns; (b) one column.

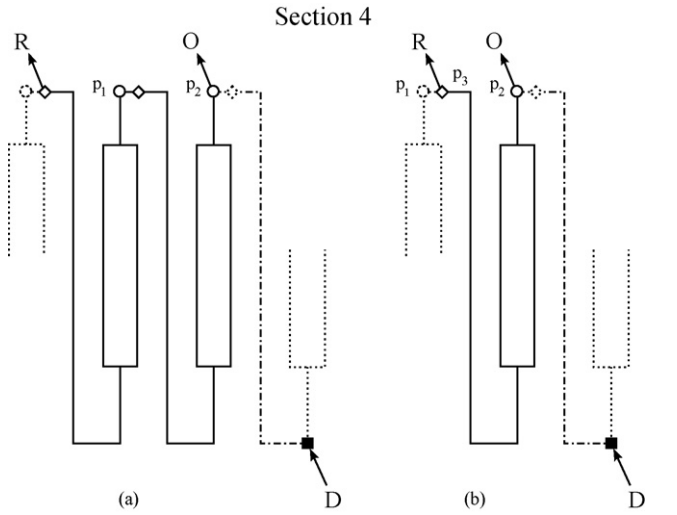

Fig. 7. Scheme of Section 4 where the O port is positioned *before* the R port: (a) two columns; (b) one column.

nent B. Therefore, pure eluent needs to be withdrawn at the Outlet port. For the analysis of Section 4 one needs to distinguish between two different possible port configurations, namely the Outlet port located after the Raffinate port or vice versa. These two configurations are shown in Figs. 6 and 7, respectively. Except for the case represented in Fig. 7(b), the regeneration requirement is fulfilled if the inequality:

$$t^* \le t^{\mathrm{r}}_{\mathrm{B},4}(\mathrm{p}_1 \text{ to } \mathrm{p}_2) \tag{20}$$

holds. However with reference to Fig. 7(b), for the configurations containing only one column in Section 4 where the Outlet port is located before the Raffinate port the residence time of the species B between p_1 and p_2 is split in two parts and the following inequality must be fulfilled:

$$t^* \le t^{\mathrm{r}}_{\mathrm{B},3}(\mathrm{p}_1 \text{ to } \mathrm{p}_3) + t^{\mathrm{r}}_{\mathrm{B},4}(\mathrm{p}_3 \text{ to } \mathrm{p}_2). \tag{21}$$

3.2.5. Summary about how to calculate the extra-column dead volume

Based on the analysis and the results above, the constraints for complete separation and regeneration can be given in terms of the effective flow rate ratios $\tilde{m}_j$. The values for V_j^{D} according to the new and the old approach can be calculated as summarized in Table 1. Using these values Eqs. (13) and (14) can be applied to any SMB configuration. In the case of nonlinear isotherms, it has already been shown that the constraints developed for SMB units without dead volume apply, provided the effective flow rate ratios $\tilde{m}_j$ are used [3].

Table 2
SMB, column and packing characteristics, and model parameters for the allene enantiomers

Column			
L (cm)			15
d_c (cm)			0.46
ϵ^*			0.63
Tubing			
V_a (mL)			0.027
V_b (mL)			0.023
V_c (mL)			0.120
Allene			
Component	H_i	$k_{s,i}a_v$ (1/s)	$\epsilon_b D_i/u$ (cm)
A	3.18	1.83	2.21×10^{-3}
B	1.66	2.70	2.21×10^{-3}

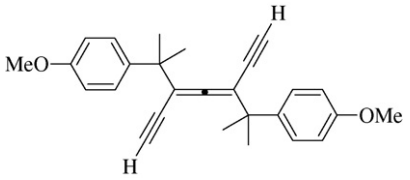

Fig. 8. Allene: (±)-3,5-bis[1-(4-methoxyphenyl)-1-methyl]hepta-3,4-diene-1,6-diyne.

4. Experimental

4.1. Materials and methods

The chiral compound used in this study and shown in Fig. 8 is one of the 1,3-diethynylallenes, which are expected to be used as modules for three-dimensional acetylenic scaffolding [6–9]. Although these allenes are axial–chiral compounds, racemic mixtures were used for scaffolding because of the difficulties in separating the enantiomers. An access to enantiomerically pure allenes is highly desirable, and in the case of (±)-3,5-bis[1-(4-methoxyphenyl)-1-methyl]hepta-3,4-diene-1,6-diyne complete separation of the racemic mixture can be achieved on laboratory HPLC–SMB unit equipped with pre-packed ChiralPak AD columns (Chiral Technologies Europe). The stationary phase is cellulose-based (amylose tris(3,5-dimethylphenylcarbamate) coated on silica support), the size of the columns is 15 cm × 0.46 cm with a particle size of 20 μm. As mobile phase, a 90/10 vol.% mixture of *n*-hexane (Merck) and 2-propanol (Fluka) was used. All experiments were carried out at room temperature, i.e. 23 ± 1 °C.

The chromatographic analysis was performed under isocratic conditions using an HPLC system (Agilent LC System 1100 Series),

Table 1
Equations to calculate the extra-column dead volume for the different possible port and column configurations, for SMBs with configuration n_1- n_2- n_3- n_4.

Dead volume	Port configuration	One column in section j	Two or more columns ($n_j \ge 2$)	Old approach for [4,5]
V_1^{D}		$V_{\mathrm{D}}^{\mathrm{i}} + V_{\mathrm{E}}^{\mathrm{o}} + \frac{Q_1}{Q_2}(V^{\mathrm{D}} - V_{\mathrm{D}}^{\mathrm{i}} - V_{\mathrm{E}}^{\mathrm{o}})$	V^{D}	$\frac{(n_1-1)V^{\mathrm{D}}+V_{\mathrm{D}}^{\mathrm{i}}+V_{\mathrm{E}}^{\mathrm{o}}}{n_1}$
V_2^{D}		V^{D}	V^{D}	$\frac{(n_2+1)V^{\mathrm{D}}-V_{\mathrm{F}}^{\mathrm{i}}-V_{\mathrm{E}}^{\mathrm{o}}}{n_2}$
V_3^{D}		$V_{\mathrm{F}}^{\mathrm{i}} + V_{\mathrm{R}}^{\mathrm{o}}$	V^{D}	$\frac{(n_3-1)V^{\mathrm{D}}+V_{\mathrm{F}}^{\mathrm{i}}+V_{\mathrm{R}}^{\mathrm{o}}}{n_3}$
V_4^{D}	O before R port	$V_{\mathrm{R}}^{\mathrm{i}} + V_{\mathrm{O}}^{\mathrm{o}} + \frac{Q_4}{Q_3}\left(V^{\mathrm{D}} - V_{\mathrm{R}}^{\mathrm{i}} - V_{\mathrm{O}}^{\mathrm{o}}\right)$	V^{D}	$\frac{n_4 V^{\mathrm{D}}+V_{\mathrm{O}}^{\mathrm{o}}-V_{\mathrm{R}}^{\mathrm{o}}}{n_4}$
	other cases	V^{D}		

V^{D}: volume of tubing parts connecting two consecutive columns.

which is equipped with a diode array UV detector, an automated data acquisition system and a multisolvent delivery system. The specification sheets of the provider (Chiral Technologies Europe) showed that in terms of retention time the columns deviate by less than 0.75% from each other. Therefore, only one column was chosen arbitrarily out of the set of available columns, and used for characterization. To determine the residence time and the overall bed void fraction of the columns, pulse injections were carried out using 1,3,5-tris-*tert*-butylbenzene (TTBB) from Fluka, which is considered to be non-retained. The residence time t_0 was determined by correcting the retention time of TTBB with the contribution of the dead volume of the HPLC. The overall void fraction of the bed ϵ^* is calculated as

$$\epsilon^* = \frac{t_0 Q}{V}. \tag{22}$$

The Henry constants of the two enantiomers were determined from the retention time of the two enantiomers when performing analytical injections.

The range of the linear adsorption behavior is determined by injecting solutions with increasing concentrations of the allene, until a shift in retention time is observed. From the results of these experiments the feed concentration for the SMB runs was fixed at 0.050 g/L of racemic solution; conditions where the enantiomers are subject to the linear isotherm:

$$n_i^* = H_i c_i. \tag{23}$$

The parameters characterizing the system are reported in Table 2.

For numerical simulations column efficiency as a functions of fluid velocity is needed. This dependence can be expressed in terms of height equivalent to a theoretical plate (HETP) with the Van Deemter equation that for a chromatographic column operated under linear conditions, can be written as follows [17]:

$$\mathrm{HETP}_i = \frac{2\epsilon_b D_i}{u} + \frac{2u}{(1-\epsilon^*)H_i k_{s,i} a_v}\left(\frac{(1-\epsilon^*)H_i}{\epsilon^* + (1-\epsilon^*)H_i}\right)^2 = \frac{2\epsilon^* D_{ap,i}}{u}, \tag{24}$$

where $D_i = \alpha_i u/2\epsilon_b$ and $k_{s,i}a_v$ are the axial dispersion and the mass transfer coefficient of each component, respectively. In this equation, the first term on the right-hand side reflects the axial dispersion in the column and the second term accounts for mass transfer; u is the superficial velocity. The parameters $\epsilon_b D_i/u$ and $k_{s,i}a_v$ can be determined by fitting Eq. (24) to the experimental points of HETP_i vs. u. The HETP_i can be determined for different fluid velocities under dilute conditions using the following equation [17]:

$$N_i = \frac{L}{\mathrm{HETP}_i} = 5.54\left(\frac{t_i^r}{W_i}\right)^2 \tag{25}$$

where N_i is the number of theoretical plates, L the length of the column, and W_i the peak width at half height. The apparent dispersion coefficient $D_{ap,i}$ to be used in Eq. (1) can be calculated according to Eq. (24). This value is different for the two components and for the individual sections due to the dependence on the fluid velocity u.

4.2. Experimental setup

The experimental setup is based on an ÄKTA™ explorer 100 system (GE Healthcare), which was modified to fulfill our requirements [18]. Our laboratory SMB unit was set up according to the geometric configuration shown in Fig. 1, and has the same location of the outlet and inlet ports in each sub-unit as shown in Fig. 2(a), (i) and (b), (i). As a result, the volume of the tubing parts a, b, and c connecting the ports and the columns is the same for all sections and corresponds to the tubing, which connects the inlet port to the column inlet (V_p^i, p = D, F), the column outlet to the outlet port (V_p^o, p = E, R, O), and the outlet port to the next inlet port ($c = V^D - V_p^i - V_p^o$), respectively. The volume of the different tubing parts, V_a, V_b and V_c, was determined by measuring the retention time of an injected pulse of TTBB (see Table 2). The ports connect the columns to the multi-position valves which are needed to control the different streams in the unit and to realize the periodic switching of the columns. Check valves (Upchurch Scientific) are installed between each pair of columns to prevent reverse flow of the fluid. Four out of the five multi-position valves are connected directly to the pumps (Feed, Desorbent, Raffinate and Extract), whereas the fifth was added to control the outlet stream O. The program controlling all the devices is based on the standard UNICORN™ software (GE Healthcare). The experiments were carried out in either the 2-2-2-2 or the 2-2-1-2 open loop configuration.

5. Results and discussion

The objective of this section is to confirm the rules to account for extra-column dead volume, as developed above. The theoretical results obtained in the previous sections are discussed and assessed by comparison with simulation results and experimental data. Altogether a set of thirteen experimental runs was performed, eight of them in the 2-2-2-2 (runs A to H) and five in the 2-2-1-2 (runs I to M) configuration. The corresponding operating conditions in terms of $\tilde{m}_j$ values and flow rates are reported in Table 3. In order to obtain precise values of the operating conditions it is of importance to

Table 3
Experimental conditions and results: A to H 2-2-2-2, I to M 2-2-1-2; switch time $t^* = 3.5$ min.

Run	Effective flow rate ratio				Flow rate (mL/min)				Purity (%)	
	$\tilde{m}_1$	$\tilde{m}_2$	$\tilde{m}_3$	$\tilde{m}_4$	Q_1	Q_2	Q_3	Q_4	Extract	Raffinate
A	3.46	1.59	2.55	1.13	1.41	0.92	1.17	0.80	97.6	100.0
B	3.44	1.64	2.60	1.10	1.40	0.93	1.18	0.79	99.0	100.0
C	3.37	1.71	2.68	1.03	1.38	0.95	1.20	0.77	– [a]	100.0
D	3.45	1.91	2.87	1.12	1.41	1.00	1.25	0.79	99.9	100.0
E	3.43	2.15	3.11	1.09	1.40	1.06	1.32	0.79	99.9	100.0
F	3.36	2.21	3.19	1.05	1.38	1.08	1.34	0.77	100.0	100.0
G	3.39	2.35	3.32	1.08	1.39	1.12	1.37	0.78	100.0	97.8
H	3.35	2.40	3.16	1.04	1.38	1.13	1.33	0.77	– [a]	100.0
I	3.43	1.90	3.00	1.12	1.40	1.00	1.25	0.79	99.8	99.5
J	3.33	2.19	3.30	1.03	1.37	1.07	1.33	0.77	99.7	96.7
K	3.43	1.89	2.79	1.04	1.40	0.99	1.20	0.77	99.8	100.0
L	3.32	2.38	3.27	1.01	1.37	1.12	1.32	0.76	100.0	99.3
M	3.40	2.45	3.34	1.08	1.39	1.14	1.34	0.78	99.8	97.6

[a] Negative peak in the chromatogram of the extract did not allow for exact purity determination.

determine the flow rates as exactly as possible. The values listed in the table were obtained by measuring the flow rates at the different ports (Feed, Desorbent, Extract, Raffinate and Outlet) throughout the entire experiment. The outlet streams were collected in small flasks over one cycle and then weighed, whilst for the inlet streams the change in weight was recorded directly with a balance. In Fig. 9, the operating points are shown in the $\bar{m}_2$– $\bar{m}_3$ plane together with the region of complete separation for the relevant linear isotherms. In all experiments, the values of $\bar{m}_1$ and $\bar{m}_4$ were fixed at specific values to fulfill the regeneration constraints. Under these conditions the SMB separation performance depends on the position of the chosen operating point in the $\bar{m}_2$– $\bar{m}_3$ plane only. Operating parameters used for the simulations are given in Table 2.

According to the equations shown in Table 1 and considering the specific position of the inlet and outlet-ports (corresponding to Fig. 2(a), (i) and (b), (i)), the extra-column dead volume that one has to consider to fulfill the constraints for complete separation is, $V^{D} = V_a + V_b + V_c$, for the 2-2-2-2 configuration, whereas for the 2-2-1-2 configuration the extra-column dead volume for Section 3 has to be $V_3^{D} = V_F^{i} + V_R^{o} = V_a + V_b$.

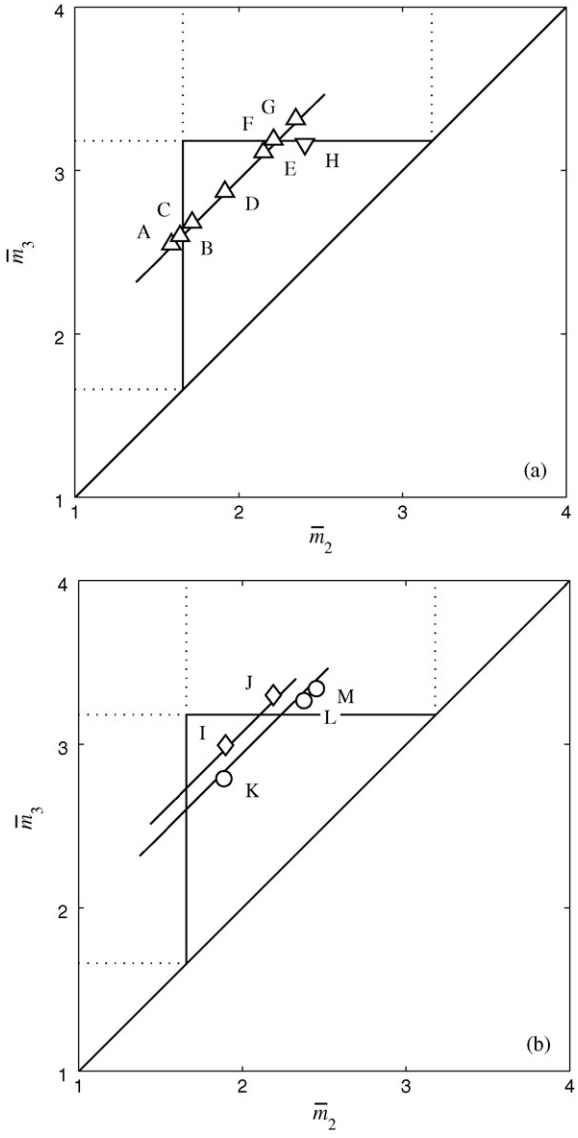

Fig. 9. Region of complete separation in the ($\bar{m}_2$, $\bar{m}_3$)plane: (a) operating points of runs A to H, 2-2-2-2 configuration; (b) operating points of runs I to M, 2-2-1-2 configuration.

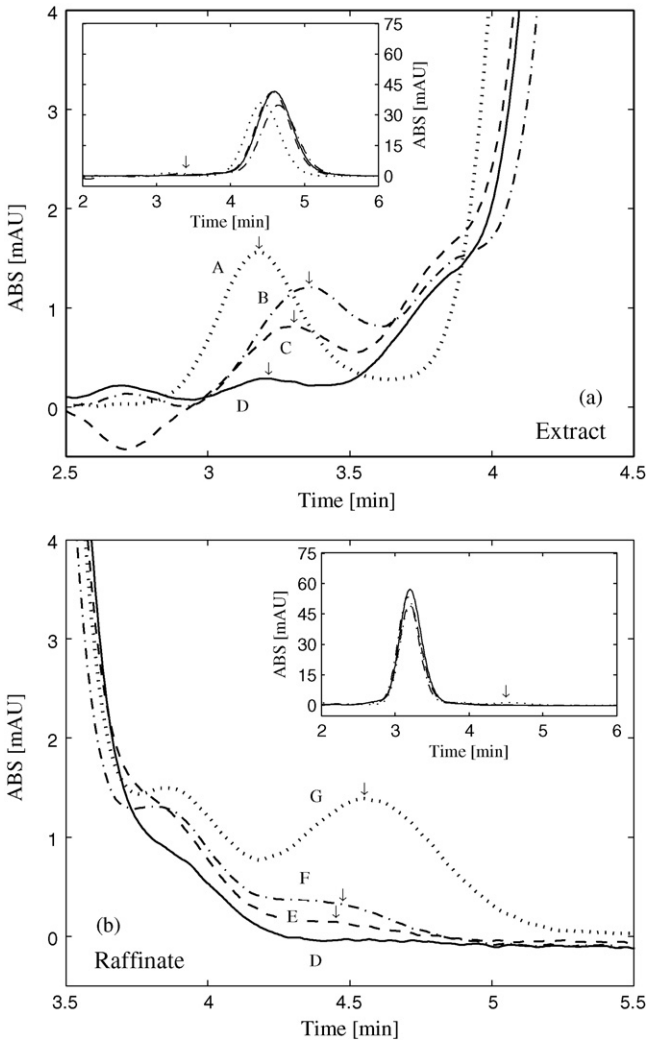

Fig. 10. Chromatograms of the product streams at steady state conditions for runs A to G. (a) Extract A to D; Run D (—); Run C (– –); Run B (– · –); Run A (· · ·); (b) Raffinate D to G; Run D (—); Run E (– –); Run F (– · –); Run G (· · ·); the arrows indicate the peaks of the impurities in Extract and Raffinate.

To verify experimentally the region of complete separation in the 2-2-2-2 case, the operating parameters of runs A to G were chosen on a line parallel in the diagonal of the $\bar{m}_2$– $\bar{m}_3$ plane. The experiments were carried out until steady state was reached; then the product streams were collected and analyzed yielding the chromatograms shown in Fig. 10. Fig. 10(a) illustrates the situation at the extract port, where it can readily be seen that from run D to A, the concentration of component B in the extract increases. On the other hand, Fig. 10(b) shows that the A impurity in the raffinate stream increases from run D to G. This behavior is in good agreement with that predicted theoretically when considering the position of the operating points with respect to the triangle boundaries as illustrated in Fig. 9(a). The chromatograms can be analyzed in terms of purities for the extract and raffinate stream, which are defined by

$$P_E = 100 \times \frac{\bar{c}_{A,E}}{\bar{c}_{A,E} + \bar{c}_{B,E}}, \qquad P_R = 100 \times \frac{\bar{c}_{B,R}}{\bar{c}_{B,R} + \bar{c}_{A,R}}, \tag{26}$$

where, $\bar{c}_{i,\alpha}$ is the average concentration of component i in the α product stream (α = R, E). The purity values listed in Table 3 were calculated from the chromatograms making use of a peak detection method that is part of the HPLC software. It becomes obvious from

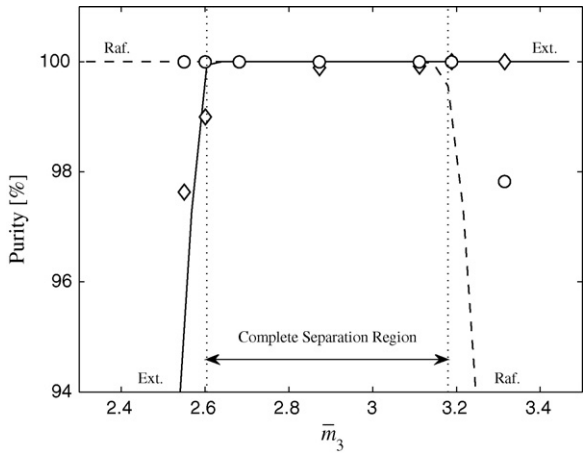

Fig. 11. Extract and Raffinate purities vs. $\bar{m}_3$ for runs A to G: experimental results for Extract (◊); simulation results for Extract (—); experimental results for Raffinate (○); simulation results for Raffinate (– –); boundaries of the region of complete separation (· · ·).

the chromatograms that an exact determination of the purities is not possible due to the shoulders of the impurities and the presence of negative peaks. Nevertheless, the trend is as expected and the lowest purities for extract and raffinate were observed at point A and G, respectively, i.e. the points that are just outside the triangle boundaries.

In Fig. 11 the experimental data are compared with the simulation results obtained using the model of Section 2.2. The simulation results indicate a steep decrease of the purities at the triangle boundaries, which qualitatively is in good agreement with the experiments. A comparison between the former approach [4,5] and the new one for the estimation of the extra-column dead volume is illustrated in Fig. 12. For the same set of experiments the $\bar{m}_3$ values are calculated twice: the previous and the present theory are represented by the filled and open symbols, respectively. For the calculation of the $\bar{m}_3$ values Eq. 13 is used for both approaches, however in the case of the former approach V_j^D is calculated differently; V_j^D is obtained by dividing the overall extra-column dead volume in section j by the number of columns in this section (see Table 1). It can be seen that the new approach improves the agreement between simulations and experiments, particularly as far as the position of the boundary for pure raffinate is concerned.

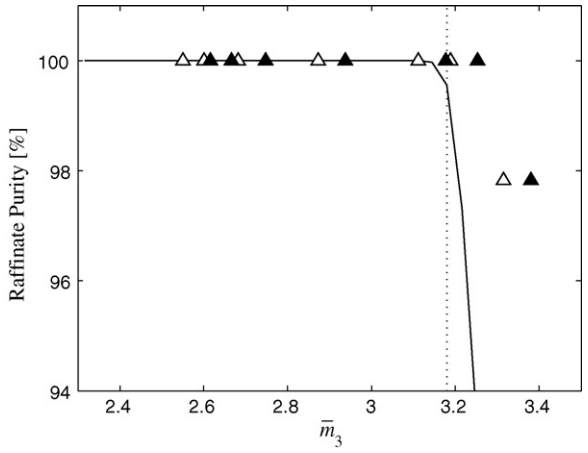

Fig. 12. Comparison of the old and new approach for runs A to H: old approach (filled symbols); new approach (open symbols); simulation results (—).

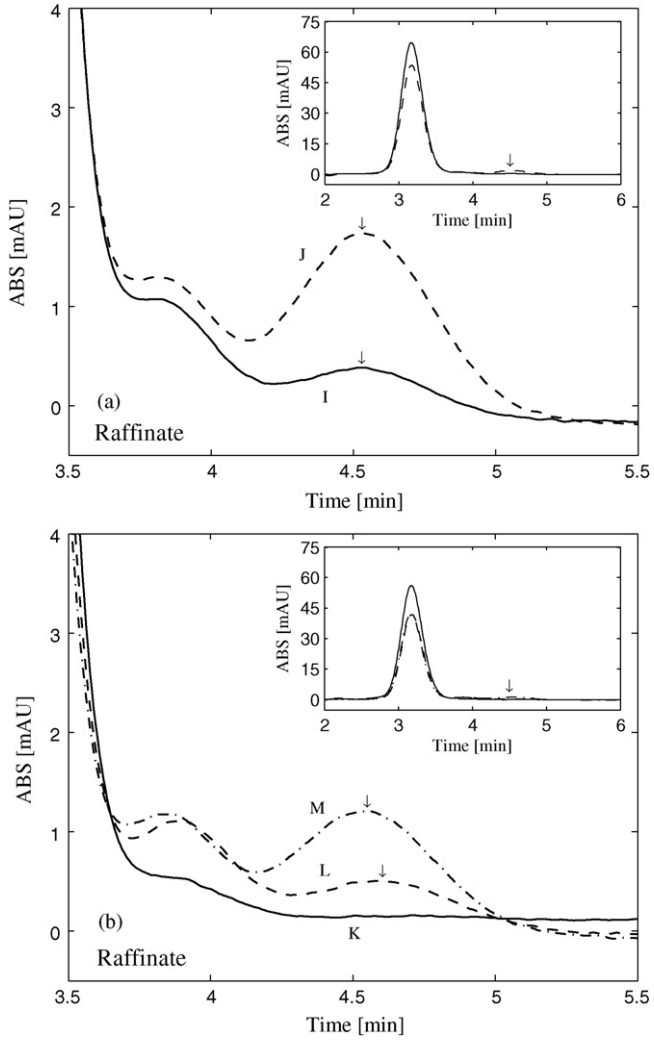

Fig. 13. Chromatograms of the product streams at steady state conditions for runs I to J and runs K to M. (a) Raffinate I to J; Run I (—); Run J (– –); (b) Raffinate K to M; Run K (—); Run L (– –); Run M (– ·–); the arrows indicate the peaks of the impurities in the Raffinate stream.

In a next step, the configuration of the unit was changed to 2-2-1-2, in order to study the effect of having one column only in Section 3(see Table 1). Due to the difference in the extra-column dead volume, even using the same flow rates and switch times, the effective flow rate ratio in Section 3 is larger for the 2-2-1-2 configuration than for the 2-2-2-2 one. Therefore, the effective flow rate ratio $\bar{m}_3$ is shifted upwards in the operating plane, although the flow rates are the same.

If this is true, then an operating point being close to or on the boundary of pure raffinate for the 2-2-2-2 configuration moves outside the region of complete separation for the 2-2-1-2 case. By running experiments using the same flow rates for the two configurations, impure raffinate should therefore be observed for the 2-2-1-2 configuration. The purity values for both raffinate and extract stream as well as the exact operating conditions are listed in Table 3. The chromatograms in Fig. 13 show that the A impurity in the raffinate stream increases from run I to J (Fig. 13(a)) and from K to M (Fig. 13(b)). These results are consistent with the position of the operating points shown in Fig. 9(b). From Table 3, it can readily be seen that runs F and J have almost the same flow rates in Sections 2 and 3; however the effective flow rate ratio $\bar{m}_3$ is larger for run J (2-2-1-2). As a consequence, the raffinate purity of run J is worse compared to the one of run F. The same conclusion is obtained,

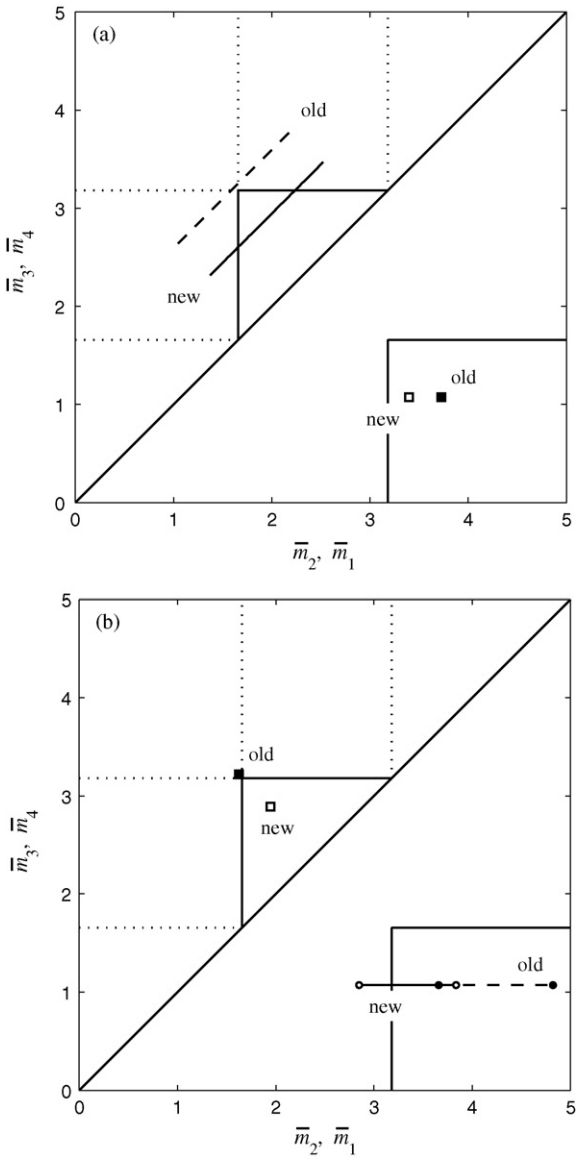

Fig. 14. Operating conditions for the simulation with large dead volume. (a) 2-2-2-2 configuration, $Q_1 = 1.528$, $Q_4 = 0.917$ mL/min and $t^* = 3.5$ min are fixed; corresponding $\bar{m}_1$ and $\bar{m}_4$ calculated with new approach (□), old approach (■); $\bar{m}_2$–$\bar{m}_3$ line calculated with new approach (—), old approach (– –). (b) 1-2-2-2 configuration, $Q_2 = 1.147$, $Q_3 = 1.395$, $Q_4 = 0.917$ mL/min and $t^* = 3.5$ min are fixed; corresponding $\bar{m}_2$ and $\bar{m}_3$ calculated with new approach (□), old approach (■); $\bar{m}_1$ line calculated with new approach (— with ◦ end), old approach (– – with • end).

when comparing run H to runs L and M. The findings are consistent with the positions of the operating points shown in Fig. 9. While the operating points F and H are located directly on the boundary of the region of complete separation, runs J, L, and M are outside due to the shift of $\bar{m}_3$.

Additionally in order to clearly illustrate the difference between the previous and the present approach and to confirm our theoretical findings simulations were performed assuming the presence of a larger dead volume. Therefore, the volume of the tubing c (V_c) was set to 0.6 mL which is five times larger than the one in our laboratory SMB unit (0.120 mL).

For the analysis of a 2-2-2-2 configuration unit with dead volume, the flow rates in Section 1 and 4 were fixed and the simulations were carried out for varying flow rates in Section 2 and 3. In Fig. 14(a), the operating conditions are shown in terms of $\bar{m}_2$ and $\bar{m}_3$. The two operating lines were calculated using the same set of flow rates; the solid and the dashed line were obtained using the present and the previous approach for the calculation of V_j^D, respectively. From Fig. 14(a), it is apparent that the dashed operating line lies outside the region of complete separation. However, as shown in Fig. 15(a), the simulation results for the extract and raffinate purities indicate a region of complete separation, whose boundaries are in good agreement with the position of the operating line calculated with the new approach.

In the case of a 1-2-2-2 configuration unit with dead volume, the flow rates were fixed in Sections 2–4 and the simulations were carried out for varying flow rates in Section 1. The operating conditions are shown in Fig. 14(b) and the purity values for both extract and raffinate stream are plotted in Fig. 15(b) as a function of the flow rate in Section 1. Again, the operating lines and points shown in Fig. 14(b) were obtained using the same set of flow rates but a different V_j^D. As indicated in Table 1, for the new approach the value of V_1^D in Section 1 depends on the flow rates in Sections 1 and 2. From Fig. 15(b), it is rather clear that only when following the new approach the behavior of the plant is described correctly. For the sake of completeness it should be mentioned that a similar simulation study could be carried for a 2-2-2-1 configuration unit with the special port configuration (Outlet port before Raffinate port) and the same conclusion could be drawn. Modeling results and experiments support the method for the calculation of extra-column dead volume presented in this work. The formulas given in

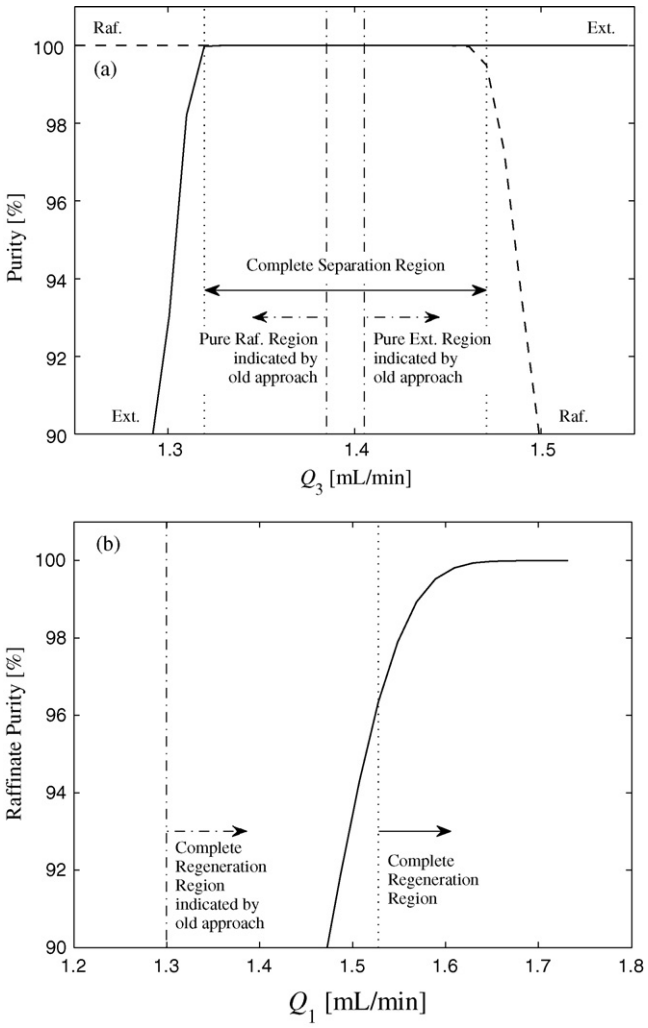

Fig. 15. (a) Simulation results for the product purities vs. Q_3 (2-2-2-2 configuration): Extract (—) and Raffinate (– –) purity. (b) Simulation results for the product purities vs. Q_1 (1-2-2-2 configuration): Extract (—) and Raffinate (– –) purity.

Table 1 should be used when designing SMB separations, together with Eq. 13 and the relevant conditions on the $\bar{m}_j$ values provided by the "Triangle Theory". We believe this is an important detail in the theory and practice of SMB separations.

Nomenclature

c_i	fluid phase concentration of component *i*
d_c	diameter of the column
$D_{ap,i}$	apparent dispersion coefficient of component *i*
D_i	axial dispersion coefficient of component *i*
D^D	dispersion coefficient in the tubing
H_i	Henry constant of component *i*
HETP	height equivalent to a theoretical plate
$k_{s,i}a_v$	mass-transfer coefficient of component *i*
L	length of the column
m_j	flow rate ratio in section *j*
$\bar{m}_j$	effective flow rate ratio in section *j*
n_i	adsorbed phase concentration of component *i*
N	number of theoretical plates
P	purity
Q_j	volumetric flow rate in section *j*
t	time coordinate
t^*	switch time
t^r	retention time
$\bar{t}^r$	effective retention time
u	superficial velocity in the column
u^D	superficial velocity in the tubing
V	volume of a column
W	peak width at half hight
z	axial coordinate
Δz	spatial grid size of the column
Δz^D	spatial grid size of the tubing

Greek letters

ϵ^*	overall bed void fraction
ϵ_b	inter particle void fraction

Subscripts and superscripts

A	component A
B	component B
i	component index
j	section index
D	dead volume

References

[1] D.-J. Wu, Y. Xie, Z. Ma, N.-H.L. Wang, Ind. Eng. Chem. Res. 37 (1998) 4023.
[2] T. Yun, G. Zhong, G. Guiochon, AIChE. J. 43 (1997) 935.
[3] C. Migliorini, M. Mazzotti, M. Morbidelli, AIChE. J. 45 (1999) 1411.
[4] M. Pedeferri, G. Zenoni, M. Mazzotti, M. Morbidelli, Chem. Eng. Sci. 54 (1999) 3735.
[5] S. Abel, G. Erdem, M. Amanullah, M. Morari, M. Mazzotti, M. Morbidelli, J. Chromatogr. A 1092 (2005) 2.
[6] M.K. ter Wiel, S. Odermatt, P. Schanen, P. Seiler, F. Diederich, Eur. J. Org. Chem. 21 (2007) 3449.
[7] R.C. Livingston, L.R. Cox, V. Gramlich, F. Diederich, Angew. Chem. Int. Ed. 40 (2001) 2334.
[8] R.C. Livingston, L.R. Cox, S. Odermatt, F. Diederich, Helv. Chem. Acta 85 (2002) 3052.
[9] M.B. Nielsen, F. Diederich, Chem. Rec. 2 (2002) 189.
[10] M. Mazzotti, G. Storti, M. Morbidelli, J. Chromatogr. A 769 (1997) 3.
[11] A. Gentilini, C. Migliorini, M. Mazzotti, M. Morbidelli, J. Chromatogr. A 805 (1998) 37.
[12] G. Hotier, R.-M. Nicoud, U.S. Patent US005578215A, 1996.
[13] G. Hotier, C. Cohen, N. Couenne, R.-M. Nicoud, U.S. Patent US005578216A, 1996.
[14] C. Migliorini, A. Gentilini, M. Mazzotti, M. Morbidelli, Ind. Eng. Chem. Res. 38 (1999) 2400.
[15] G. Guiochon, J. Choromatgr. A 965 (2002) 129.
[16] G. Guiochon, A. Felinger, D.G. Shirazi, A.M. Katti, Fundamentls of Preparative and Nonlinear Chromatography, 2nd ed., Academic Press, New York, 2006.
[17] M.D. LeVan, G. Carta, C.M. Yon, Perry's Chemical Engineers' Handbook, 7th ed., McGrow-Hill, New York, 1997, Section 16.
[18] S. Abel, M.U. Bäbler, C. Arpagaus, M. Mazzotti, J. Stadler, J. Chromatogr. A 1043 (2004) 201.